GPR Modeling for Rapid Characterization of Layered Media

Subrata Maiti[1, *], Sarat K. Patra[1], and Amitabha Bhattacharya[2]

Abstract—The success of a ground penetrating radar (GPR) signal modeling scheme largely depends on its accuracy and computational efficiency. Most of the modeling schemes suffer from inaccuracy because of unrealistic assumptions of complex GPR environment. In this respect full wave model (FWM) of GPR signal is a promising approach for accurate characterization of multi-layered media. However, large computation time of FWM compared to other simplified models makes the approach inefficient for real time application. In this work an FWM scheme is developed based on electric field equivalent magnetic current density at antenna phase center. The compact analytical expression of Green's function representing response due to layered media is derived. Then a plane wave model (PWM) is proposed by introducing a spreading factor based on simplified expression of the FWM. The model inversion is successfuly carried out by a gradient based algorithm. A stepped frequency continuous wave GPR in off-ground monostatic configuration is implemented in laboratory environment to verify performances of the models. Experimental analysis proves that the proposed PWM is as accurate as FWM, and its computation efficiency is enormous to detect layered media parameters.

1. INTRODUCTION

Estimation of electrical and geometrical properties of layered media by ground penetrating radar (GPR) technique finds many applications [1, 2] in the fields of civil engineering, archaeology, geology, military, etc. Monostatic GPR is useful for achieving high scanning speed [3, 4]. The accuracy and scanning speed are important requirements for an efficient GPR system. There is always compromise between these important performance parameters to formulate a modeling scheme based on GPR application requirement. The numerical modeling [5–8] can take care of the complex geometry and its boundary conditions. However, they often suffer from low computational efficiency leading to difficulty in real time implementation. Analytical modeling can be applied under simplified hypotheses on the nature of the structure, resulting in problem specific solution. The common midpoint (CMP) method [9–11], based on wave propagation speed is a popular approach used for GPR signal analysis. But it suffers from processing delay as it requires several traces for single profile measurement. Spectral inversion method proposed by [12, 13] is proven to be successful for estimating electrical parameters of the layered media with low conductivity profile. This method is based on common reflection method with assumption of plane wave propagation. Full wave models (FWM) are more promising schemes for accurate estimation of media properties [14, 15]. Here 3-D Maxwell's equations are solved to find the Green's function due to sub-surface media. In the field of off-ground monostatic stepped frequency continuous wave (SFCW) GPR, Lambot et al. [14] have contributed significantly by introducing concept of linear transfer function (LTF) model and an FWM scheme for characterization of multi-layered media. The scheme is successfully used for estimating and monitoring soil water content [16]. However, computation efficiency of this model is poor compared to other simplified models based on plane wave assumption. Many researchers are proposing layer stripping (LS) techniques [4, 17, 18] for fast characterization of layered

[1] Department of Electronics and Communication Engineering, National Institute of Technology, Rourkela, Odisha-769008, India.
[2] Department of Electronics and Electrical Communication Engineering, Indian Institute of Technology, Kharagpur, West Bengal-721302, India.

media. The drawbacks of these techniques are inaccuracy due to signal dispersion and accumulation of error due to recursive formulation [18].

    In this work, an FWM is formulated based on scattered reflected field due to electric field equivalent magnetic current source at antenna phase center. Then a plane wave model (PWM) is proposed based on common reflection mehtod and simplified expression of the FWM. By introducing a spreading factor, the PWM becomes as accurate as FWMs without altering its speed of computation. A comprehensive analysis on the PWM and FWMs established that they are highly correlated. An SFCW GPR is implemented with help of a vector network analyzer (VNA) and a TEM horn antenna in laboratory. The GPR detection performance of the proposed model is compared with [14] by testing a single layered wet sand and a two layered media.

2. FORMULATION OF GPR SIGNAL MODEL

2.1. Modeling Assumption

The SFCW radar is emulated with help of a VNA and an antenna in monotstatic off-ground configuration. For far field measurement, the antenna is assumed to be a point source and receiver located at its phase center. The signal is assumed to be propagating in normal direction only, i.e., in z directions. The VNA, antenna and sub-surface are modeled as linear systems [14] in series and parallel as shown in Fig. 1(a). By applying Masson's gain formula, the VNA measured complex reflection coefficient $S_{11}(\omega)$ is expressed as following.

$$S_{11}(\omega) = \frac{Y(\omega)}{X(\omega)} = H_i(\omega) + \frac{H_t(\omega)\, G_{xx}^\uparrow(\omega) H_r(\omega)}{1 - H_f(\omega)\, G_{xx}^\uparrow(\omega)} \tag{1}$$

where $X(\omega)$ is the transmitted signal and $Y(\omega)$ is the received signal at the VNA reference plane; $H_i(\omega)$, $H_t(\omega)$, $H_r(\omega)$ and $H_f(\omega)$ are the return loss, transmit transfer function, receive transfer function, and feedback loss transfer function respectively for the antenna. $G_{xx}^\uparrow(\omega)$ is the Green's function representing the air-subsurface media. All these frequency dependent transfer functions can be evaluated by suitable calibration process as mentioned in [19]. The air-subsurface media is modeled as multi-layered media (shown in Fig. 1(b)) where any nth layer is homogeneous and is characterized by its electric permittivity (ϵ_n), electric conductivity (σ_n), magnetic permeability (μ_n) and thickness (h_n). The permeability μ_n is assumed to be free space value μ_0. The soil materials are significantly dispersive because of frequency dependency of effective dielectric constant ($\epsilon_e = \sigma + i\omega\epsilon$). The frequency dependency is usually described by the Debye relaxation equation [20] as given below.

$$\epsilon_e(f) = \epsilon_{e,\infty} + \frac{\epsilon_{e,0} - \epsilon_{e,\infty}}{1 + j\frac{f}{f_r}} \tag{2}$$

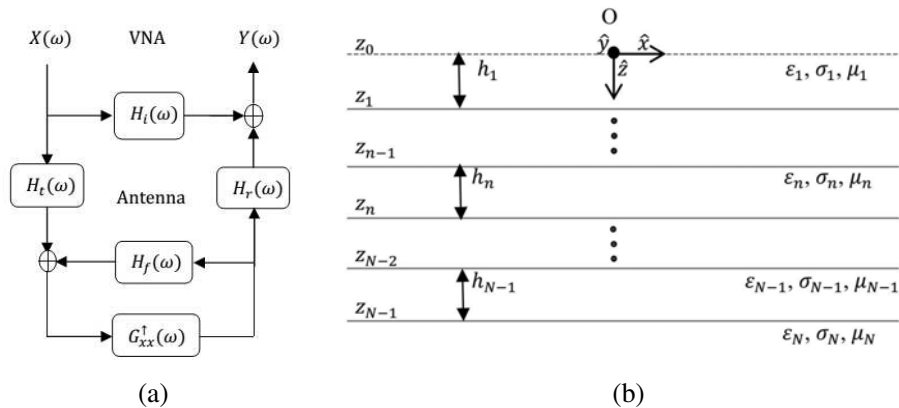(a)   (b)

Figure 1. (a) Block diagram representing the VNA-antenna-multilayered medium system [14], (b) model configuration of N-layered medium with a point source.

where f is the frequency and f_r is the relaxation frequency of the material, $\epsilon_{e,0}$ is the static permittivity, and $\epsilon_{e,\infty}$ is the permittivity at infinite frequency. Over the limited operating frequency, ϵ can be assumed to be constant and σ as a linear function of frequency as given below.

$$\sigma\left(f\right) = \sigma_c + \sigma_r\left(f - f_c\right) \tag{3}$$

where σ_c is the static electric conductivity (S/m) at center frequency f_c of the frequency band and σ_r the linear variation rate (S/m/GHz) with frequency.

2.2. Derivation of FWM

The source and receiver part of the antenna is located at the antenna phase center at the origin O of the coordinate system. For TEM horn antenna, the transmitted electric field E_{xp}^t is assumed to be directing towards x-direction only. Applying Huygen's principle [21, pp. 575–581], the equivalent magnetic current density $\mathbf{M}^s$ is expressed as following.

$$\mathbf{M}^s = -2\hat{\mathbf{n}} \times \hat{\mathbf{x}}E_{xp}^t = -2E_{xp}^t\hat{\mathbf{y}} \tag{4}$$

and equivalent electric current density

$$\mathbf{J}^s = 0 \tag{5}$$

The $\hat{\mathbf{n}}$ is acting towards the direction of EM wave propagation (in z-direction). The radiated far field due to this equivalent magnetic source is to be derived by solving Maxwell's equations. The Green's function $G_{xx}^{\uparrow}(\omega)$ is defined as the ratio between back scattered x-directed electric field and transmitted x-directed electric field at antenna phase center at frequency ω rad/s. The spatial domain Green's function at the source point $((x, y, z) = 0)$ is obtained from the spectral domain Green's function $\tilde{G}_{xx}^{\uparrow}(k_\rho, \omega)$ as

$$G_{xx}^{\uparrow}(0, \omega) = \frac{1}{4\pi} \int\limits_0^{+\infty} \tilde{G}_{xx}^{\uparrow}\left(k_\rho, \omega\right) k_\rho dk_\rho \tag{6}$$

The integration variable k_ρ is a spectral domain parameter. After a rigorous mathematical analysis by following [22–25], the analytical expression of the spectral domain Green's function is derived (see Appendix A) and its final form is given below.

$$\tilde{G}_{xx}^{\uparrow}\left(k_\rho, \omega\right) = \left[R_n^{TE} - R_n^{TM}\right]e^{-2\Gamma_n h_n} \tag{7}$$

where R_n^{TM} and R_n^{TE} are transverse magnetic global reflection coefficient and transverse electric global reflection coefficient respectively accounting for all reflections from the multi-layered interfaces as given in [23, pp. 48–53].

$$R_n^{TM} = \frac{r_n^{TM} + R_{n+1}^{TM}\exp(-2\Gamma_{n+1}h_{n+1})}{1 + r_n^{TM}R_{n+1}^{TM}\exp(-2\Gamma_{n+1}h_{n+1})} \tag{8}$$

$$r_n^{TM} = \frac{\eta_{n+1}\Gamma_n - \eta_n\Gamma_{n+1}}{\eta_{n+1}\Gamma_n + \eta_n\Gamma_{n+1}} \tag{9}$$

$$R_n^{TE} = \frac{r_n^{TE} + R_{n+1}^{TE}\exp(-2\Gamma_{n+1}h_{n+1})}{1 + r_n^{TE}R_{n+1}^{TE}\exp(-2\Gamma_{n+1}h_{n+1})} \tag{10}$$

$$r_n^{TE} = \frac{\mu_{n+1}\Gamma_n - \mu_n\Gamma_{n+1}}{\mu_{n+1}\Gamma_n + \mu_n\Gamma_{n+1}} \tag{11}$$

$\Gamma_n\left(= \sqrt{k_\rho^2 - k_n^2}\right)$ is vertical wave number of nth layer, k_n is free space propagation constant of nth layer with relation $k_n^2 = -\zeta_n\eta_n$, $\zeta_n = i\omega\mu_n$, and $\eta_n = \sigma_n + i\omega\epsilon_n$. Here h_1 is the thickness of the air media i.e., the height of the antenna phase center from the ground surface located at z_1. Ideally the height h_1 should be function of frequency as the location of antenna phase center changes with frequency. However, the antenna phase center can be placed at a fixed location like at the center of the antenna aperture. A study by Jadoon et al. [26] proved that the linear transfer function model used to represent

the antenna behavior inherently accounts for the gain and delay due to frequency dependent antenna phase center location through the calibration process.

By assuming TEM horn antenna as an infinitesimal x-directed electric dipole, the spectral domain Green's function [14] is obtained as following.

$$\tilde{G}_{xx}^{\uparrow}(k_\rho, \omega) = \left[R_n^{TM} \frac{\Gamma_n}{\eta_n} - R_n^{TE} \frac{\zeta_n}{\Gamma_n} \right] e^{-2\Gamma_n h_n} \tag{12}$$

Let us denote this FWM [14] as FWM-1 and the proposed one in Eq. (7) as FWM-2.

2.3. Formulation of PWM Based on Simplified Formula of FWM

Common reflection method based on plane wave propagation is found in various literatures [1, 12] and it is mostly applied for approximate estimation of the layered media's electrical parameters while conductivity is negligible. Here this method is modified to make it very accurate to estimate both conductivity and dielectric constant without altering its computational efficiency. For plane wave propagation, reflection coefficient $(r_{n,n+1})$ at any nth layer interface (z_n) is given by following relation.

$$r_{n,n+1} = \frac{Z_{n+1} - Z_n}{Z_{n+1} + Z_n} \tag{13}$$

Z_n is the impedance of nth layer media given by

$$Z_n = \sqrt{\frac{\zeta_n}{\eta_n}} = \sqrt{\frac{i\omega\mu_n}{\sigma_n + i\omega\epsilon_n}} \tag{14}$$

Any nth layer media propagation parameter (γ_n) is expressed as

$$\gamma_n = \alpha_n + i\beta_n = \sqrt{i\omega\mu_n(\sigma_n + i\omega\epsilon_n)} = \sqrt{\zeta_n\eta_n} = ik_n \tag{15}$$

where α_n and β_n are attenuation and phase constants respectively for nth layer media. The first order reflection $(\hat{r}_{n,n+1}^1)$ from nth interface (z_n) is given by

$$\left(\hat{r}_{n,n+1}^1 \right) = r_{n.n+1} \prod_{j=1}^{n-1} \left(1 - (r_{j,j+1})^2 \right) \prod_{j=1}^{n} \exp\left(-2\gamma_j h_j \right) \tag{16}$$

Plane wave propagation is possible when source is in infinite distance from the media. For finite distance case, Eq. (16) needs to be modified to make it accurate. Here FWM-2 expression represented by Eqs. (6) and (7) is simplified and important findings are used to modify the common reflection method to derive the PWM.

Let us consider the case of two-layered media. A two-layered media can be created with half space air media $(\sigma_1 = 0$ and $\epsilon_{r1} = 1)$ followed by a media having either conductivity (σ_2) infinity or thickness (h_2) infinity. From Eqs. (6) and (7) we can write.

$$G_{xx}^{\uparrow}(\omega) = \frac{1}{4\pi} \int_0^{+\infty} \left[R_1^{TE} - R_1^{TM} \right] e^{-2\Gamma_1 h_1} k_\rho dk_\rho \tag{17}$$

Here $\Gamma_1 = \sqrt{k_\rho^2 - k_1^2} = \sqrt{k_\rho^2 + \gamma_1^2}$ and the expression of global reflection coefficients for TE and TM can be obtained as $R_1^{TE} = r_1^{TE}$ and $R_1^{TM} = r_1^{TM}$ from Eqs. (8)–(11). Therefore, Eq. (17) is modified to

$$G_{xx}^{\uparrow}(\omega) = \frac{1}{4\pi} \int_0^{+\infty} \left[r_1^{TE} - r_1^{TM} \right] e^{-2h_1\sqrt{k_\rho^2 + \gamma_1^2}} k_\rho dk_\rho \tag{18}$$

It can be observed in Eq. (18) that $e^{-2h_1\sqrt{k_\rho^2 + \gamma_1^2}}$ is highly oscillation function and $\left[r_1^{TE} - r_1^{TM} \right]$ changes slowly with respect to the integration variable k_ρ. Now applying method of stationary phase [23, pp.

79–82], integration in Eq. (18) can be simplified as following.

$$G_{xx}^{\uparrow}(\omega) = \frac{r_{1,2}}{2\pi} \int\limits_{0}^{+\infty} e^{-2h_1\sqrt{k_\rho^2+\gamma_1^2}} k_\rho dk_\rho \tag{19}$$

Note that $\frac{d}{dk_\rho}(\sqrt{k_\rho^2+\gamma_1^2}) = 0$ at $k_\rho = 0$. Again at $k_\rho = 0$, $r_1^{TE} = r_{1,2} = -r_1^{TM}$, where $r_{1,2}$ is TEM wave reflection coefficient at z_1 interface for normal incidence as defined in Eq. (13). Now applying integration by parts repeatedly Eq. (19) is simplified to

$$G_{xx}^{\uparrow}(\omega) = \frac{r_{1,2}}{2\pi} \left[\frac{e^{-2\gamma_1 h_1}}{2\frac{h_1}{\gamma_1}} + \frac{e^{-2\gamma_1 h_1}}{4(h_1)^2} \right] \tag{20}$$

Now let us consider the case of three layered media. In this case R_1^{TE} and R_1^{TM} can be expressed as following.

$$R_1^{TE} = \frac{r_1^{TE} + R_2^{TE}\exp(-2\Gamma_2 h_2)}{1 + r_1^{TE}R_2^{TE}\exp(-2\Gamma_2 h_2)} = \frac{r_1^{TE} + r_2^{TE}\exp(-2\Gamma_2 h_2)}{1 + r_1^{TE}r_2^{TE}\exp(-2\Gamma_2 h_2)} = r_1^{TE} + r_2^{TE}\left(1 - r_1^{TE2}\right) e^{-2\Gamma_2 h_2} + \dots \tag{21}$$

and

$$R_1^{TM} = \frac{r_1^{TM} + R_2^{TM}\exp(-2\Gamma_2 h_2)}{1 + r_1^{TM}R_2^{TM}\exp(-2\Gamma_2 h_2)} = \frac{r_1^{TM} + r_2^{TM}\exp(-2\Gamma_2 h_2)}{1 + r_1^{TM}r_2^{TM}\exp(-2\Gamma_2 h_2)} = r_1^{TM} + r_2^{TM}\left(1 - r_1^{TM2}\right) e^{-2\Gamma_2 h_2} + \dots \tag{22}$$

Now Eq. (17) can be written as

$$G_{xx}^{\uparrow}(\omega) = \frac{1}{4\pi} \int\limits_{0}^{+\infty} \left[\left(r_1^{TE} - r_1^{TM}\right) + \left\{ r_2^{TE}\left(1 - r_1^{TE2}\right) - r_2^{TM}\left(1 - r_1^{TM2}\right) \right\} e^{-2\Gamma_2 h_2} + \dots \right] e^{-2\Gamma_1 h_1} k_\rho dk_\rho \tag{23}$$

Rearranging the terms we get

$$G_{xx}^{\uparrow}(\omega) = \frac{1}{4\pi} \int\limits_{0}^{+\infty} \left[r_1^{TE} - r_1^{TM} \right] e^{-2\Gamma_1 h_1} k_\rho dk_\rho$$

$$+ \frac{1}{4\pi} \int\limits_{0}^{+\infty} \left[r_2^{TE}\left(1 - r_1^{TE2}\right) - r_2^{TM}\left(1 - r_1^{TM2}\right) \right] e^{-2(\Gamma_1 h_1 + \Gamma_2 h_2)} k_\rho dk_\rho + Higher\ order\ terms \tag{24}$$

Again by applying method of stationary phase followed by integration by parts, Eq. (24) can be simplified as following.

$$G_{xx}^{\uparrow}(\omega) = \frac{r_{1,2}}{2\pi} \left\{ \frac{1}{2\frac{h_1}{\gamma_1}} + \frac{1}{4(h_1)^2} \right\} e^{-2\gamma_1 h_1}$$

$$+ \frac{r_{2,3}\left(1 - r_{1,2}^2\right)}{2\pi} \left\{ \frac{1}{2\left(\frac{h_1}{\gamma_1} + \frac{h_2}{\gamma_2}\right)} + \frac{\left(\frac{h_1}{\gamma_1^3} + \frac{h_2}{\gamma_2^3}\right)}{4\left(\frac{h_1}{\gamma_1} + \frac{h_2}{\gamma_2}\right)^3} \right\} e^{-2(\gamma_1 h_1 + \gamma_2 h_2)} + Higher\ order\ terms \tag{25}$$

Note that terms with higher than h^2 variation are neglected from the analytical expression of the integration with highly oscillating term as given below.

$$\int\limits_{0}^{+\infty} e^{-2(\Gamma_1 h_1 + \Gamma_2 h_2)} k_\rho dk_\rho = e^{-2(\gamma_1 h_1 + \gamma_2 h_2)} \left[\frac{1}{2\left(\frac{h_1}{\gamma_1} + \frac{h_2}{\gamma_2}\right)} + \frac{\left(\frac{h_1}{\gamma_1^3} + \frac{h_2}{\gamma_2^3}\right)}{4\left(\frac{h_1}{\gamma_1} + \frac{h_2}{\gamma_2}\right)^3} + \dots \right] \tag{26}$$

In Eq. (25), the 1st term signifies contribution due to 1st order reflection $(R_{1,2}^1)$ from interface z_1.

$$R_{1,2}^1 = \frac{r_{1,2}}{2\pi} \left\{ \frac{1}{2\frac{h_1}{\gamma_1}} + \frac{1}{4(h_1)^2} \right\} e^{-2\gamma_1 h_1} = \frac{\hat{r}_{1,2}^1}{2\pi} \left\{ \frac{1}{2\frac{h_1}{\gamma_1}} + \frac{1}{4(h_1)^2} \right\} \tag{27}$$

where $\hat{r}_{1,2}^1$ expression is given by Eq. (16). The superscript of $R_{1,2}^1$ denotes the order of reflection coefficient. Similarly the 2nd term signifies contribution due to 1st order reflection $(R_{2,3}^1)$ from interface z_2.

$$R_{2,3}^1 = \frac{\hat{r}_{2,3}^1}{2\pi} \left\{ \frac{1}{2\left(\frac{h_1}{\gamma_1} + \frac{h_2}{\gamma_2}\right)} + \frac{\left(\frac{h_1}{\gamma_1^3} + \frac{h_2}{\gamma_2^3}\right)}{4\left(\frac{h_1}{\gamma_1} + \frac{h_2}{\gamma_2}\right)^3} \right\} \tag{28}$$

Based on simplified expressions found in Eqs. (20) and (25) for two and three layered media respectively and using Eq. (16), the expression for 1st order reflection from z_n can be generalized as following.

$$R_{n,n+1}^1 = \left(\frac{\hat{r}_{n,n+1}^1}{2\pi i}\right) \left(\frac{1}{2\sum\limits_{j=1}^{n} h_j/\gamma_j} + \frac{\left(\sum\limits_{j=1}^{n} h_j/\gamma_j^3\right)}{4\left(\sum\limits_{j=1}^{n} h_j/\gamma_j\right)^3} \right) \tag{29}$$

One complex term 'i' is introduced at the denominator of the expression (29) to have phase matching between Eqs. (16) and (29). All the higher order reflections due to multiple reflections at interface z_2 can be obtained by following Eq. (29). As an example the mth order reflections from z_2 can be found as following.

$$R_{2,3}^m = \frac{\hat{r}_{2,3}^1}{2\pi i}(r_{2,1}r_{2,3})^{(m-1)} e^{-(m-1)2\gamma_2 h_2} \left\{ \frac{1}{2\left(\frac{h_1}{\gamma_1} + m\frac{h_2}{\gamma_2}\right)} + \frac{\left(\frac{h_1}{\gamma_1^3} + m\frac{h_2}{\gamma_2^3}\right)}{4\left(\frac{h_1}{\gamma_1} + m\frac{h_2}{\gamma_2}\right)^3} \right\} \tag{30}$$

Eq. (30) can also be derived by considering mth order term in Eq. (25). With h^2 variation insignificant, Eq. (29) can be modified as following.

$$R_{n,n+1}^1 = \left(\frac{\hat{r}_{n,n+1}^1}{2\pi i}\right) \left(\frac{1}{\sum\limits_{j=1}^{n} 2h_j/\gamma_j} \right) \tag{31}$$

The generalized formula for $R_{n,n+1}^m$ i.e., mth order reflection from interface z_n can be obtained by solving Eqs. (6)–(11) and finding terms corresponding to $(r_{1,2}^{a_1} r_{2,3}^{a_2} \ldots r_{n,n+1}^{a_n})$. Here a_i are +Ve integer constants related by $\sum_{i=1}^{n} a_i = m$ and $a_n \geq 1$. The overall Green's function due to N-layered media with maximum order of reflection N_o can be expressed as

$$G_{xx}^{\uparrow PWM}(\omega) = \sum_{i=1}^{N_o} \sum_{k=1}^{N-1} R^i{}_{k,k+1} \tag{32}$$

The N_o value should be decided best on accuracy requirement of the GPR system. Let us denote this model (32) as plane wave model (PWM). The $G_{xx}^{\uparrow PWM}$ obtained by considering only h variation term is denoted as PWM-1 and PWM-2 for considering both h and h^2 variations. With no integration required to compute $G_{xx}^{\uparrow PWM}$ compared to FWMs, the proposed PWM schemes are very time efficient.

3. ANALYSIS AND INVERSION OF MODEL

3.1. Analysis of Models

A comprehensive analysis has been carried out for all the models in terms of correlation between Green's functions in frequency and time domain over wide range of parameter vector space. The correlation coefficient ($corr\_coff$) between two real vectors $\mathbf{X}$ and $\mathbf{Y}$ is defined as

$$corr\_coff = \frac{\sum\limits_{i=1}^{N_f}(x_i - \bar{x})(y_i - \bar{y})}{\sqrt{\sum\limits_{i=1}^{N_f}(x_i - \bar{x})^2 \sum\limits_{i=1}^{N_f}(y_i - \bar{y})^2}} \tag{33}$$

where x_i, y_i are the elements of vectors $\mathbf{X}$ and $\mathbf{Y}$ respectively, and $\bar{x}$ and $\bar{y}$ are mean values. N_f is the number of frequency points and is taken as 101 here with spacing of 40 MHz over the frequency band of 0.5 to 4.5 GHz. Parameters values are varied exponentially to compute total 4851 (11 along ϵ_r, 21 along σ and 21 along h) iterations for comparing all types of Green's functions over the wide parameter vector space ($2 < \epsilon_r < 101$; $10 < \sigma < 10^4$ mS/m; $1 < h < 10^3$ cm). It is observed that the Green's functions of FWM-1 [14] and FWM-2 differ by a constant amplitude factor and a phase shift of 180°. After compensating the phase shift and performing correlation analysis it is found that both the models are highly correlated with correlation coefficients between G_{xx}^{FWM-1} and G_{xx}^{FWM-2} almost 1 (> 0.9999841) for real parts as well as for imaginary parts. Correlation coefficient between time domain Green's functions is found to be greater than 0.9999899. Therefore FWM-1 and FWM-2 can be treated as one model with similar behavior in frequency and time domain. Next PWMs are compared with FWM-2. For PWMs, the order of reflection (N_o) is varied from 5 to 25 with observation that G_{xx}^{PWM} doesn't change as N_o is increased above 20 on the selected range of parameter vector space. Since PWMs differ with FWM-2 by 90° as seen in Eqs. (29) and (31), the FWM-2 Green's function is multiplied by $-1i$ before performing correlation coefficients matrices. The results of analysis are presented in Table 1. It also includes averaged %RMS difference between the Green's functions defined by following formula.
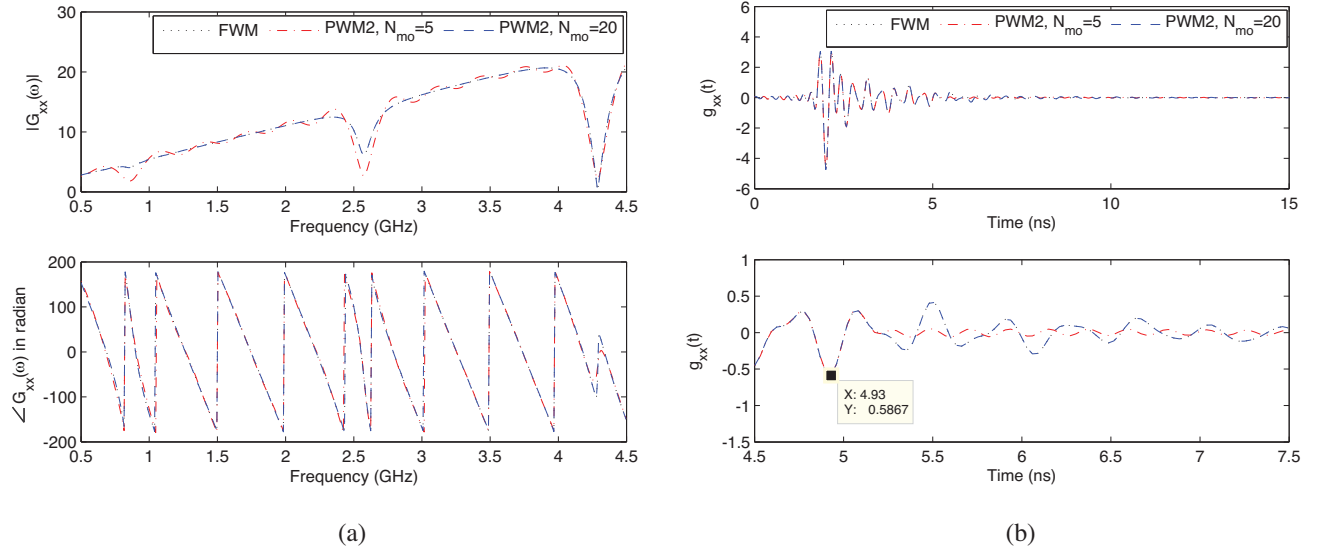
$$\%RMS\_diff = 100 \times \sqrt{\frac{\sum\limits_{i=1}^{N_f}\left|\left(G_{xx}^{\uparrow PWM}(\omega_i)\right) - \left(G_{xx}^{\uparrow FWM-2}(\omega_i)\right)\right|^2}{\sum\limits_{i=1}^{N_f}\left|\left(G_{xx}^{\uparrow FWM-2}(\omega_i)\right)\right|^2}} \tag{34}$$

Only the worst case values of $corr\_coff$ between time domain Greens's functions and $\%RMS\_diff$ between frequency domain Green's functions obtained for ϵ_r values 2, 16 and 81 over σ-h plane are presented. It shows that PWMs and FWM-2 are highly correlated as we consider for h^2 variation and higher value of N_o. Similar results are obtained when PWMs are compared with FWM-1. The time required to compute single Green's functions over 101 frequency points and averaged over 1000 times running in an 1.93 GHz core i3 laptop are presented in last row of Table 1. The results prove that the PWMs are extremely time efficient compared to FWMs. The FWM-1 with SFCW radar based on VNA platform is rigorously analyzed for uniqueness, stability, noise performances [19, 27]. It is expected that the FWM-2 and PWMs will have similar noise and stability performance as they are highly correlated with FWM-1.

In order to explain how the spreading term for higher order reflection looks, a synthetic model of two layered media ($\epsilon_{r1} = 0$, $\sigma_1 = 0$, $h_1 = 35$ cm, $\epsilon_{r2} = 81$, $\sigma_2 = 10$ mS/m, $h_2 = 1$ cm) is chosen for which worst case correlation between PWM and FWM is observed. Fig. 2 explains how PWM2 Green's function becomes closer to the FWM as order of reflection coefficient (N_o) is increased from 5 to 20. For $N_o = 5$, amplitude difference between PWM and FWM is clearly observed in frequency domain plot, and this difference is observed after 5th order reflection in time domain plot. As for $N_o = 20$, these differences are minimal as observed in the plots.

Table 1. Comparison of Models in terms of $\%RMS\_diff$, $Corr\_coff$ and timing efficiency.

ϵ_r	Max $\%RMS\_diff$ with FWM-2 in σ-h plane				Min $Corr\_coff$ with FWM-2 in σ-h plane			
	PWM-1		PWM-2		PWM-1		PWM-2	
	$N_o = 5$	$N_o = 20$	$N_o = 5$	$N_o = 20$	$N_o = 5$	$N_o = 20$	$N_o = 5$	$N_o = 20$
2	4.4075	4.4096	0.1376	0.1351	0.9991483	0.9991476	0.9999995	0.9999995
16	6.0538	2.6394	5.5798	0.0674	0.9980958	0.9996207	0.9984172	0.9999998
81	21.2627	2.5535	21.127	0.6580	0.9803440	0.9996406	0.9806714	0.9999815

Processing time of $G_{xx}(\omega)$ in milliseconds					
PWM-1		PWM-2		FWM-1	FWM-2
6.2414	6.9968	6.3512	8.6450	2280.0	2278.2

Figure 2. Plot of Green's functions ($G_{xx}(\omega)$) for the synthetic model of two layered media in (a) frequency domain and (b) in time domain.

3.2. Inversion Approach

The estimation of subsurface media parameters by inverse modeling is a nonlinear problem. By formulating the inverse problem in least-squares sense, the objective function can be defined as following.

$$\Phi(\mathbf{b}) = \left| G_{xx}^{\uparrow*}(\omega) - G_{xx}^{\uparrow}(\omega, \mathbf{b}) \right|^T \left| G_{xx}^{\uparrow*}(\omega) - G_{xx}^{\uparrow}(\omega, \mathbf{b}) \right| \tag{35}$$

where $G_{xx}^{\uparrow*}(\omega)$ are the vectors containing measured, and $G_{xx}^{\uparrow}(\omega, \mathbf{b})$ are the vectors containing simulated Green's function of the layered media. The parameter vector $\mathbf{b}$ (consists of $\mu_n, \epsilon_n, \sigma_n, h_n$) needs to be estimated by minimizing the objective function $\Phi(\mathbf{b})$ in Eq. (35). The objective function for all the models, i.e., FWMs and PWMs are highly non linear having multiple minimas over the parmater vector space. A layer stripping technique (LS) is utilized to get preliminary information of layer thickness and electrical parameters and then gradient based algorithm of Matlab software is used to optimize the objective function. By LS method the properties of the multi layered media is recursively estimated by resolving one layer at a time starting from the top layer. A brief description is presented to describe the approach.

3.3. Layer Stripping (LS)

In this method, analysis of the GPR signal is done in time domain. Let us assume that the parameters for 1st to nth layer are known. Neglecting presence of multiple reflections, the parameters of $(n+1)$th layer media can be extracted by following steps as given below.

Step 1. Extracting $\epsilon_{r,n+1}$ and h_{n+1}: Synthetically generate a Green's function for a PEC placed at z_n interface by using Eq. (31). Find the peak A_n^{pc} due to the PEC by taking IFFT of the frequency domain Green's function. For PEC at z_n, $r_{n,n+1} = -1$. Now comparing PEC reflection A_n^{pc} with the 1st order reflection A_n from z_n interface of the layered media under test, following expression can be written based on Eq. (13).

$$-\frac{A_n}{A_n^{pc}} = r_{n,n+1} = \frac{Z_{n+1} - Z_n}{Z_{n+1} + Z_n} \tag{36}$$

Now $\mu_r = 1$ for all the layers and $\epsilon_{r,n}$ and σ_n are known. Neglecting conductivities of both the layers i.e., σ_n and σ_{n+1}, $\epsilon_{r,n+1}$ of $(n+1)$th layer media can be evaluated from Eq. (36). Then find thickness h_{n+1} of $(n+1)$th layer media by relation

$$h_{n+1} = -\frac{c \times (t_{n+1} - t_n)}{2\beta_{n+1}/\beta_1} \tag{37}$$

where β_1 is the propagation constant of free space, and t_n and t_{n+1} are the time of arrival for 1st order reflection from the interfaces z_n and z_{n+1}, respectively. For $\sigma_{n+1} = 0$, Eq. (37) is simplified to

$$h_{n+1} = -\frac{c \times (t_{n+1} - t_n)}{2\sqrt{\epsilon_{r,n+1}}} \tag{38}$$

Step 2. Extracting σ_{n+1} and updating h_{n+1} and σ_{n+1}: Now synthetically generate a Green's function for a (n+1) layer media bounded by PEC at bottom by using Eq. (31). Find 1st order $(n+1)$th peak i.e., reflection A_{n+1}^{pc} due to z_{n+1} interface by taking IFFT of the frequency domain Green's function. Now ratio of A_{n+1}^{pc} with A_n can be written based on Eq. (31) as following.

$$\frac{A_{n+1}^{pc}}{A_n} = \left(\frac{1 - r_{n,n+1}^2}{-r_{n,n+1}}\right) \frac{\sum_{j=1}^{n} h_j/\gamma_j}{\sum_{j=1}^{n+1} h_j/\gamma_j} \exp\left(-2\alpha_{n+1}h_{n+1}\right) \tag{39}$$

Neglect σ_{n+1} to calculate $\sum_{j=1}^{n+1} h_j/\gamma_j$. Now α_{n+1} can be approximated at center frequency as

$$\alpha_{n+1} = \frac{\sigma_{c,n+1}}{2\sqrt{\epsilon_{r,n+1}}} Z_1 \tag{40}$$

where $\sigma_{c,n+1}$ is the effective conductivity of $(n+1)$th layer at center frequency (f_c) and Z_1 the free space impedance. Now $\sigma_{c,n+1}$ can be evaluated by solving Eq. (39) after replacing α_{n+1} from Eq. (40). Then update the thickness h_{n+1} of $(n+1)$th layer media by relation (37) and using the newly obtained value of $\sigma_{c,n+1}$. Repeat the step 2 few times as long as $\sigma_{c,n+1}$ and h_{n+1} settle to almost constant values with pre defined accuracy.

4. RESULTS AND DISCUSSION

4.1. Experimental Setup

The SFCW radar setup presented in Fig. 3 is assembled with a VNA (E5071C of Agilent), TEM horn antenna (BBHA 9120A, Schwarzbeck Mess-Elektronik) and a wooden tank ($138.5\,\text{cm} \times 98.5\,\text{cm} \times 30\,\text{cm}$) containing material under test. A metal plate ($122\,\text{cm} \times 81\,\text{cm}$) is kept at the bottom of the tank to control the boundary condition. The whole setup was kept at the roof top in outdoor environment without control of environment temperature, humidity. VNA and cable connecting the antenna was calibrated by standard OSM kit to bring the reference measurement plane at cable and antenna interface.
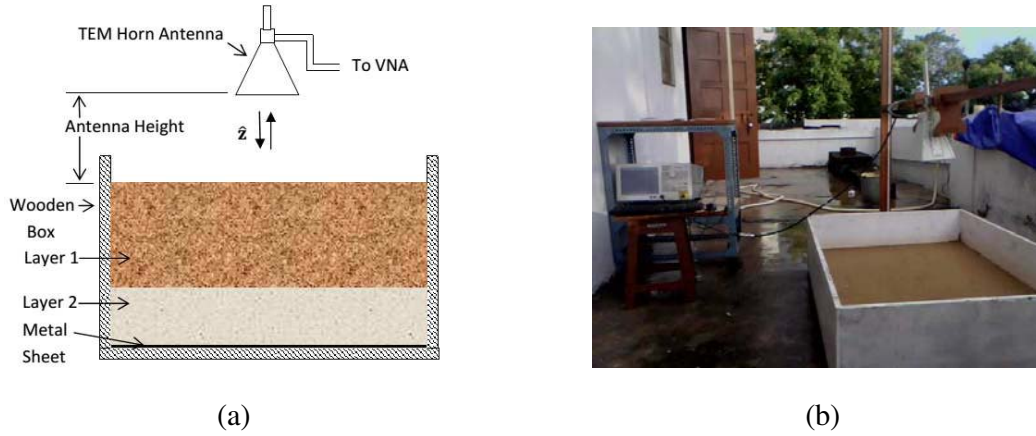
Figure 3. (a) Model of the laboratory experimental setup and (b) experimental setup at the roof top.

The frequency range from 800 MHz to 4000 MHz was swept with frequency step of 4 MHz. During GPR calibration we need to measure $S_{11}(\omega)$ while keeping antenna aperture on different heights above the metal plate. Due to manual adjustment of the antenna stand, our height measurement inaccuracy was around ± 2 mm.

4.2. GPR Calibration

First the experimental GPR system was calibrated by taking reflection coefficient $S_{11}(\omega)$ measurements with antenna at different heights above a large size metal plate following the process mentioned in [19]. Plot for the various transfer functions (LTFs) and extracted Green's functions for metal plate placed at different heights are presented in Fig. 4. Fig. 4(a) presents the plot for antenna reflection coefficients $H_i(\omega)$ obtained by calibration process as well as three free space measurements. Fig. 4(b) presents the plot of feedback loss transfer function ($H_f(\omega)$). In Fig. 4(c), $H(\omega)$ ($= H_t(\omega)H_r(\omega)$) magnitude and phase are plotted. Finally Fig. 4(d) presents the amplitude plots of extracted Green's functions for metal plates placed at different heights. Theoretically (from Eq. (31)) the Green's function $G_{xx}(\omega)$ for metal plate should be proportional to frequency and inversely proportional to the antenna height. However, it can be observed that $G_{xx}(\omega)$ for different heights fluctuate a lot with crossing each other. Since effect of millimetre inaccuracy of height measurements are more towards high frequency, fluctuation of $G_{xx}(\omega)$ are more towards higher frequencies. The effect of calibration error is also observed in the plots of $H_i(\omega)$ with difference between calibrated and free space measurement data increasing towards high frequencies. This error limits the usable bandwidth [19] for GPR detection. Based on optimum GPR detection performance, the bandwidth from 0.9 to 2.1 GHz is selected for GPR processing.

4.3. Detection of Single Layered (1L) Sand

A single layered media was created in the laboratory environment by placing wet sand in the wooden box. At the bottom there is a metal plate to form a PEC boundary. The sand layer was prepared homogeneously with uniform thickness of approximate 10 cm. After the GPR experiment, simulation was conducted for all the modeling schemes to estimate the sand's electrical parameters. The total number of parameters to be estimated here are 5 i.e., height of the antenna from sand surface (h_1), sand layer thickness (h_2), its relative dielectric constant (ϵ_{r2}), conductivity (σ_{c2}) at center frequency (f_c) and conductivity variation coefficients (σ_{r2}). For both the PWMs, maximum up to 5th order reflection was considered to calculate the Green's function. The Table 2 presents the results of GPR inversion and frequency averaged %RMS error of Green's function after optimization. It can be observed that PWMs are as accurate as FWMs to estimate electrical and geometrical parameters of single layered sand. Resulted %RMS errors are comparable with small difference in fraction number. The timing efficiency gained by PWMs are enormous. Further the LS has yielded approximate values for the media

parameters. Fig. 5 presents plot of measured and modeled Green's function in frequency and time domain. Here FWM Green's functions are multiplied by appropriate complex constants to normalize and phase synchronise with PWMs. It can be observed that the phase response is reproduced well by model inversion. However, there is significant amplitude error resulting in RMS error between measured and modeled Green's function. The RMS error is largely contributed by the calibration error due to manual height measurement inaccuracy of the test setup. The time domain plot shows very good agreement between measured and modeled Green's function even for the higher order reflection coefficients.

4.4. Detection of Two Layered (2L) Media

A two-layered media was created in the laboratory environment by placing wood powder above the same wet sand layer used for single layer testing. Thickness of wood powder layer was approximately 20.5 cm. As usual metal sheet was kept below the wet sand layer. The total number of parameters estimated here are 7 i.e., 1st layer thickness (h_2), relative dielectric constants (ϵ_{r2} and ϵ_{r3}), conductivities (σ_{c2} and σ_{c3}) at center frequency (f_c) and conductivity variation coefficients (σ_{r2}, σ_{r3}). Antenna height (h_1) from surface of 1st layer and 2nd layer thickness (h_3) were taken as known parameters and were fixed at manual measurement values 33 cm and 10 cm respectively. For both the PWMs maximum up to 5th order reflection from the interface z_2 and up to 2nd order reflection from z_3 are considered to calculate the Green's function. The GPR estimation results are presented in the Table 3. As usual it is observed that PWMs are highly time efficient compared to the FWMs. Very good similarities are observed among the estimated layer parameters by all four models. However, with percentage RMS errors higher than
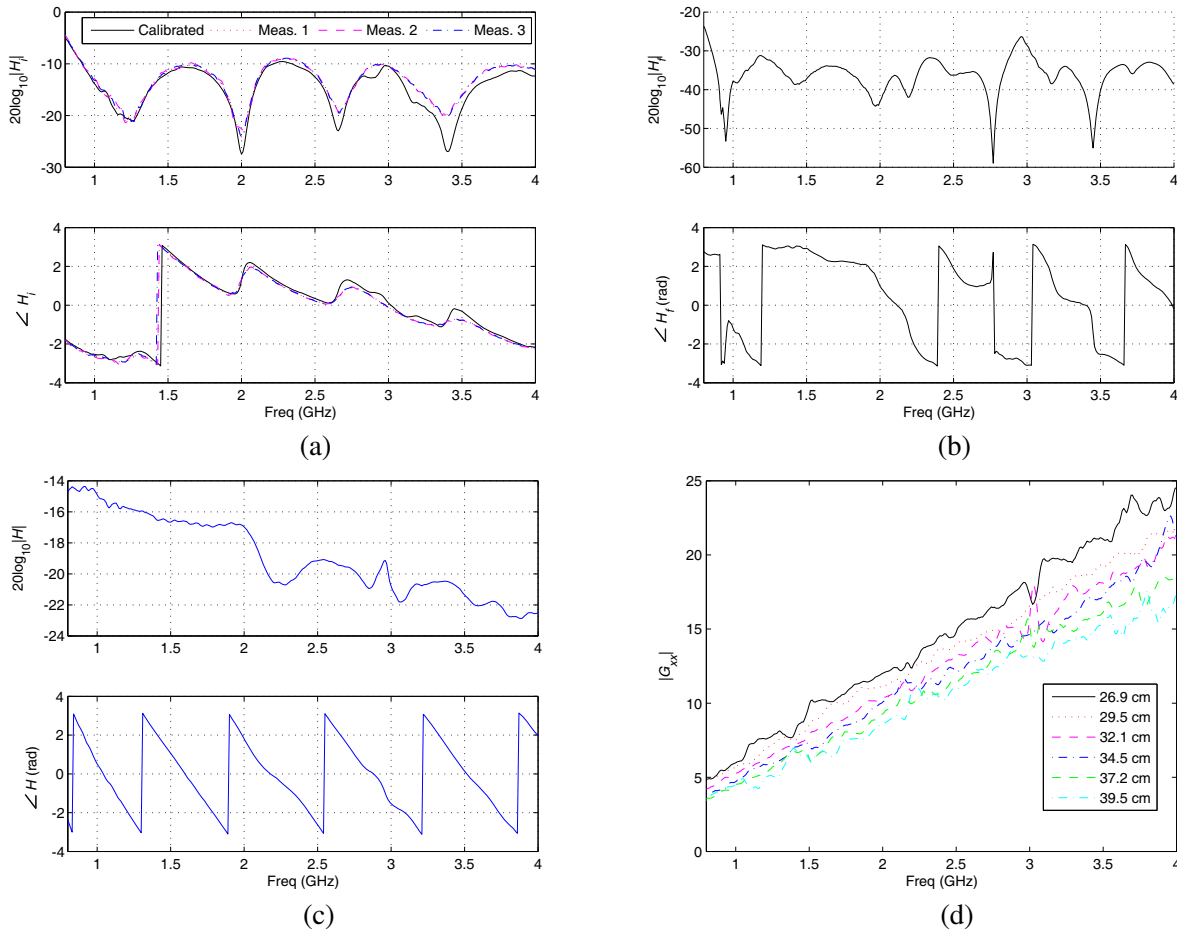

Figure 4. LTF parameters extracted by calibration.

Table 2. Results of GPR estimation with single layered wet sand.

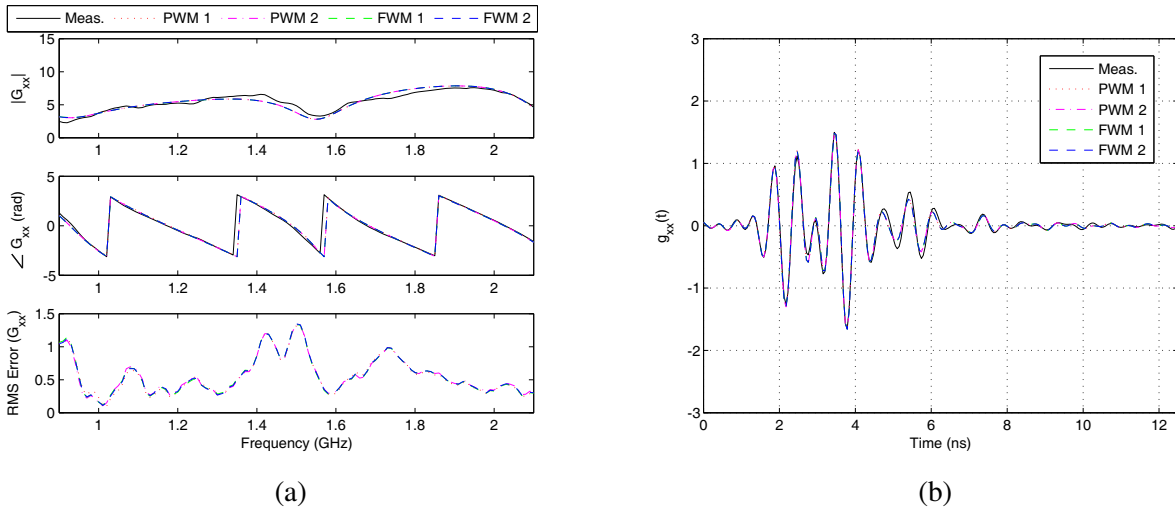| Model	Estimated Sand Layer Parameters						
used	h_1	h_2	ϵ_{r2}	σ_{c2}	σ_{r2}	Run	%RMS
	(cm)	(cm)		(mS/m)	(mS/m/GHz)	time(s)	error
LS	32.5002	9.1113	6.7848	15.3203	–	0.8327	–
PWM-1	32.3315	10.0780	5.7825	17.0768	22.1853	0.3433	11.0198
PWM-2	32.3281	10.0553	5.8220	17.1302	22.3376	0.2865	11.0485
FWM-1	32.3271	10.0209	5.8583	17.2685	22.2603	136.33	11.0663
FWM-2	32.3279	10.0714	5.7990	17.1518	22.0697	90.96	11.0848

Figure 5. Compare measured and modeled Green's functions for single layered wet sand in (a) frequency domain and (b) in time domain.
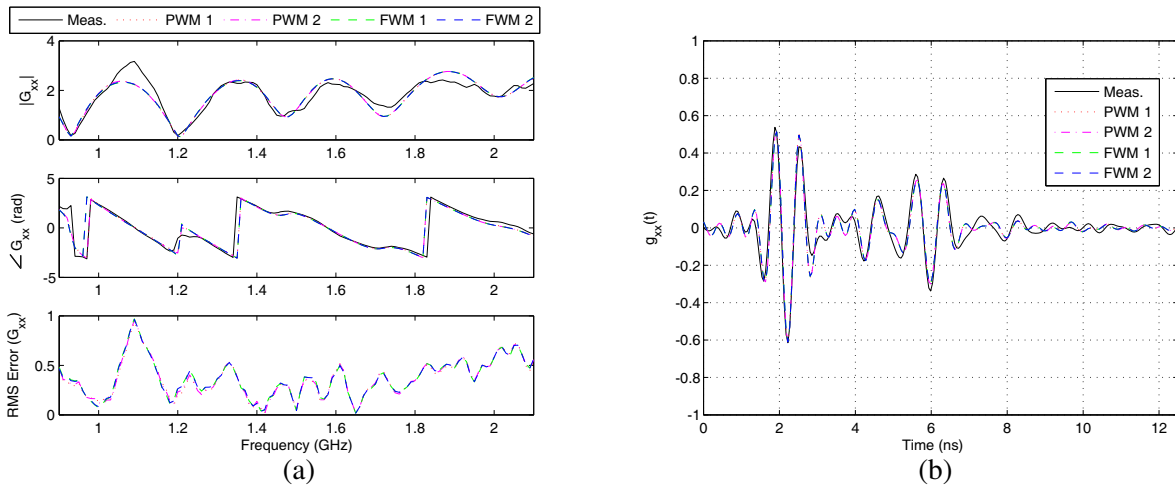

Figure 6. Compare measured and modeled Green's functions for two layered media in (a) frequency domain and (b) in time domain.

Table 3. Results of GPR estimation with two layered media.

Model used	h_2 (cm)	ϵ_{r2}	ϵ_{r3}	σ_{c2} (mS/m)	σ_{r2} (mS/ m/GHz)	σ_{c3} (mS/m)	σ_{r3} (mS/ m/GHz)	Run time(s)	%RMS error
					Estimated Sand Layer Parameters				
LS	21.5188	2.4532	5.7867	17.4788	–	79.5612	–	1.1686	–
PWM-1	20.4694	2.3304	6.2386	26.4405	20.4477	23.6606	28.3045	0.4655	21.5407
PWM-2	20.5096	2.3255	6.2488	26.2595	20.6708	23.8719	27.2110	0.4436	21.7214
FWM-1	20.4226	2.3412	6.2638	26.0235	22.7457	25.4625	20.2707	352.53	21.9360
FWM-2	20.4925	2.3258	6.2612	25.9421	22.4331	25.1261	20.7312	232.07	21.8701

21 for all the models, it is quite possible that models inversions yield error in parameter estimation. By comparing Table 2 and Table 3 for wet sand parameters, it can be observed that inverted ϵ_r values are changed by maximum up to 8% and much higher changes are observed for conductivities (σ) values. Due to manual setup, uniform thickness and homogeneity of two-layered media could not be obtained. The imperfect model of two-layered media along with calibration inaccuracy majorly contributes to such a high amount of RMS error. The plots of measured and the modeled Green's functions in frequency and time domain are presented in Fig. 6. Similar errors for frequency response and time response for Green's functions are observed across all the models.

4.5. Discussion

The efficiency of PWMs depends on the choice of maximum order of reflections N_o. N_o value should be decided based on compromise between accuracy and speed requirement as well as the range of wide parameters vector space over which GPR estimation needs to be carried out. Without doing a comprehensive analysis, the choices of N_o values can be justified by comparing the average %RMS error performance of PWMs with FWMs. The GPR experiments on 1L and 2L media have shown the advantage of PWM schemes over FWMs in terms of speed of computation. Though the timing efficiency achieved by PWMs is enormous compared to FWMs, both types of models require evaluation of linear transfer functions by time consuming calibration process. The future works need to address this issue.

5. CONCLUSIONS

We propose an SFCW monostatic GPR based on a fast and accurate modeling scheme called PWM which can reconstruct the electrical and geometrical parameters of layered media. Analysis data and laboratory experiments show that the proposed PWM closely matches with FWM resulting accuracy of GPR detection as good as FWM schemes. The proposed layer stripping approach has potential to resolve the layered media parameters including conductivities approximately. This helps the gradient based approach to work efficiently to invert the model for single layered and two layered media. Clearly the proposed integrated approach gives a valuable alternative for efficient characterization of layered media. With low detection time for two layered media, this inverse modeling approach can be suitable for real time GPR applications. Future works will focus on to simplify the process of calibration and extend the model for more number of layers.

APPENDIX A. COMPUTATION OF THE SPECTRAL DOMAIN GREEN'S FUNCTION $G_{\mathbf{XX}}^{\uparrow}(\mathbf{K_\rho}, \boldsymbol{\omega})$

Scattering field computation due to layered media for various types of sources is treated by authors as in [22–25]. Here multi-layered media in Fig. 1(b) is placed at the far field of the antenna. We wish to compute the reflected scattered fields (**E**, **H**) at the receiver antenna phase center ($r(x, y, z) = 0$) due

to specified current distributions ($\mathbf{J}$, $\mathbf{M}$) at transmitter antenna phase center. These fields are governed by the Maxwell's equations, and its time harmonic differential form [28] are given below.

$$\nabla \times \mathbf{H} - \eta(\omega)\mathbf{E} = \mathbf{J}^s \tag{A1}$$

$$\nabla \times \mathbf{E} + \zeta(\omega)\mathbf{H} = -\mathbf{M}^s \tag{A2}$$

$\zeta(\omega)$ and $\eta(\omega)$ are the media's EM parameters defined as $\zeta(\omega) = j\omega\mu$ and $\eta(\omega) = \sigma + j\omega\epsilon$. $\mathbf{J}^s$ and $\mathbf{M}^s$ denote electric and magnetic specific source currents respectively, and they are located at the origin of the Cartesian coordinate system. The time dependence is implicit with an $\exp(j\omega t)$ dependence in the formulation. For multi-layered horizontal media distributed over infinite length and width it is easier to solve the fields in spectral domain by splitting them into a set of transverse electric (TE) fields and another set of transverse magnetic (TM) fields. The Fourier transformation of a scalar function $f(x,y)$ with respect to the transverse coordinates is defined as

$$\tilde{f}(\mathbf{k}_T) = \int_{-\infty}^{+\infty}\int_{-\infty}^{+\infty}\exp(j\mathbf{k}_T.\mathbf{x}_T)f(\mathbf{x}_T)\,dxdy \tag{A3}$$

where $\mathbf{k}_T = \{k_x, k_y\}$ and $\mathbf{x}_T = \{x, y\}^T$. Let us introduce the horizontal vector partial derivative, $\partial_T = \{\partial_x, \partial_y\}$, and $\partial_T = -j\mathbf{k}_T$. From Eqs. (4) and (5) it is clear that there is only magnetic current source for which we need to solve the reflected electric field. In a homogeneous media the Maxwell's equations Eqs. (A1) and (A2) can be written in spectral domain as

$$\partial_z\hat{\mathbf{z}} \times \tilde{\mathbf{H}} - j\mathbf{k}_T \times \tilde{\mathbf{H}} - \eta\tilde{\mathbf{E}} = 0 \tag{A4}$$

$$\partial_z\hat{\mathbf{z}} \times \tilde{\mathbf{E}} - j\mathbf{k}_T \times \tilde{\mathbf{E}} + \zeta\tilde{\mathbf{H}} = -\tilde{\mathbf{M}}^s \tag{A5}$$

These equations can be separated in terms of TE and TM forms, and transverse components can be expressed as summation of contributions due to TE and TM fields. The vertical component of the electric and magnetic fields are found by solving modified Helmholtz equation as following.

$$\tilde{E}_z = \hat{\mathbf{z}}.\left(j\mathbf{k}_T \times \tilde{\mathbf{M}}_T^s\right)\tilde{G}(z) \tag{A6}$$

$$\tilde{H}_z = \left\{-\eta\tilde{M}_z^s - \zeta^{-1}\partial_z\left(j\mathbf{k}_T \cdot \tilde{\mathbf{M}}_T^s - \partial_z\tilde{M}_z^s\right)\right\}\tilde{G}(z) \tag{A7}$$

where

$$\tilde{G}(z) = \frac{\exp(-\Gamma|z|)}{2\Gamma}, \tag{A8}$$

$\Gamma = \left(\mathbf{k}_T.\mathbf{k}_T + \gamma^2\right)^{\frac{1}{2}}$, $\gamma^2 = \eta\zeta$. After some steps of derivations, the horizontal components of the electric field are expressed as following.

$$\tilde{\mathbf{E}}_T = -\frac{j\mathbf{k}_T}{k_\rho^2}\partial_z\tilde{E}_z + \frac{\zeta}{k_\rho^2}\left(j\mathbf{k}_T \times \hat{\mathbf{z}}\tilde{H}_z + \hat{\mathbf{z}} \times \tilde{\mathbf{M}}_T^s\right) \tag{A9}$$

Keeping the separation of TE and TM modes and substituting Eqs. (A6) and (A7) in Eq. (A9), the final expression of electric field is obtained as following.

$$\tilde{\mathbf{E}} = \tilde{G}^{TMMJ}\tilde{\mathbf{M}}^s + \tilde{G}^{TEMJ}\tilde{\mathbf{M}}^s \tag{A10}$$

where $\tilde{M}^s = \left\{\tilde{M}_x^s, \tilde{M}_y^s, \tilde{M}_z^s\right\}^T$ and

$$\tilde{G}^{TMMJ} = \begin{pmatrix} \dfrac{-jk_xjk_y\Gamma sign(z)}{k_\rho^2} & \dfrac{jk_xjk_x\Gamma sign(z)}{k_\rho^2} & 0 \\[3mm] \dfrac{-jk_yjk_y\Gamma sign(z)}{k_\rho^2} & \dfrac{jk_xjk_y\Gamma sign(z)}{k_\rho^2} & 0 \\[3mm] -jk_y & jk_x & 0 \end{pmatrix}, \tag{A11}$$

$$\tilde{G}^{TEMJ} = \begin{pmatrix} \dfrac{jk_xjk_y\Gamma sign(z)}{k_\rho^2} & \dfrac{jk_yjk_y\Gamma sign(z)}{k_\rho^2} & jk_y \\[3mm] \dfrac{-jk_xjk_x\Gamma sign(z)}{k_\rho^2} & \dfrac{-jk_xjk_y\Gamma sign(z)}{k_\rho^2} & -jk_x \\[3mm] 0 & 0 & 0 \end{pmatrix} \tag{A12}$$

Since there is only y-directed magnetic source term $\tilde{M}_y^s$, the general solution for the vertical electric and magnetic fields in the region $(0 < z < z_1)$ are written as

$$\tilde{E}_z = \frac{jk_x \tilde{M}_y^s}{2\Gamma} \left[\exp\left(-\Gamma_1 z\right) + R_1^{TM} \exp\left(\Gamma_1 \left(z - 2z_1\right)\right) \right] \tag{A13}$$

$$\tilde{H}_z = \frac{jk_y \tilde{M}_y^s}{2\zeta} \left[\exp\left(-\Gamma_1 z\right) + R_1^{TE} \exp\left(\Gamma_1 \left(z - 2z_1\right)\right) \right] \tag{A14}$$

For the monostatic SFCW radar with single TEM horn antenna, the emitter and receiver both are assumed to be located at the antenna phase center at $z = 0$. By substituting Eqs. (A13) and (A14) in Eq. (A9) the x-directed electric field at phase center is computed as

$$\tilde{E}_{x,z=0} = \frac{1}{2k_\rho^2} \left[-2\zeta - k_\rho^2 \right] \tilde{M}_y + \frac{1}{2k_\rho^2} \left[k_x^2 R_1^{TM} - k_y^2 R_1^{TE} \right] \exp\left(-2\Gamma_1 z_1\right) \tilde{M}_y \tag{A15}$$

Considering only the backscattered field $(\tilde{E}_{x,z=0}^r)$ and using the relation $\mathbf{M}^s = -2E_{xp}^t \hat{\mathbf{y}}$ from Eq. (4), Eq. (A15) is simplified to

$$\tilde{E}_{x,z=0}^r = \frac{1}{2k_\rho^2} \left[k_x^2 R_1^{TM} - k_y^2 R_1^{TE} \right] \exp\left(-2\Gamma_1 z_1\right) \left(-2\tilde{E}_{xp}^t\right) \tag{A16}$$

Accordingly, the response due to the multilayered medium is defined as following.

$$\tilde{G}_{xx}^\uparrow \left(k_\rho, \omega\right) = \frac{\tilde{E}_{x,z=0}^r}{\tilde{E}_{xp}^t} = \frac{1}{k_\rho^2} \left[k_y^2 R_1^{TE} - k_x^2 R_1^{TM} \right] \exp\left(-2\Gamma_1 z_1\right) \tag{A17}$$

Transforming to polar coordinate Eq. (A17) is modified to

$$\tilde{G}_{xx}^\uparrow \left(k_\rho, \omega\right) = \left[J_0 \left(k_\rho \rho\right) \left\{ R_1^{TE} - R_1^{TM} \right\} + J_2 \left(k_\rho \rho\right) \cos 2\theta \left\{ R_1^{TE} + R_1^{TM} \right\} \right] e^{-2\Gamma_1 h_1} \tag{A18}$$

where $\theta = \arctan(\frac{y}{x})$, $h_1 = z_1 - z_0$ is the thickness of 1st layer media. For monostatic configuration, the 1st layer is the air media. For the specific monostatic configuration ($\rho = 0$), the Green's function is further simplified to a single integral as given below.

$$\tilde{G}_{xx}^\uparrow \left(k_\rho, \omega\right) = \left[R_1^{TE} - R_1^{TM} \right] e^{-2\Gamma_1 h_1} \tag{A19}$$

REFERENCES

1. Daniels, D. J., *Ground Penetrating Radar*, The Institution of Engineering and Technology, London, UK, 2007.
2. Annan, A., "Gprhistory, trends, and future developments," *Subsurface Sensing Technologies and Applications*, Vol. 3, No. 4, 253–270, 2002.
3. Gentili, G. G. and U. Spagnolini, "Electromagnetic inversion in monostatic ground penetrating radar: TEM horn calibration and application," *IEEE Transactions on Geoscience and Remote Sensing*, Vol. 38, No. 4, 1936–1946, 2000.
4. Loizos, A. and C. Plati, "Accuracy of ground penetrating radar horn-antenna technique for sensing pavement subsurface," *IEEE Sensors Journal*, Vol. 7, No. 5, 842–850, 2007.
5. Belli, K., C. M. Rappaport, H. Zhan, and S. Wadia-Fascetti, "Effectiveness of 2-D and 2.5-D FDTD ground-penetrating radar modeling for bridge-deck deterioration evaluated by 3-D FDTD," *IEEE Transactions on Geoscience and Remote Sensing*, Vol. 47, No. 11, 3656–3663, 2009.
6. Atteia, G. E. and K. F. A. Hussein, "Realistic model of dispersive soils using PLRC-FDTD with applications to GPR systems," *Progress In Electromagnetics Research B*, Vol. 26, 335–359, 2010.
7. Millington, T. M. and N. J. Cassidy, "Optimising GPR modelling: A practical, multi-threaded approach to 3D FDTD numerical modelling," *Computers & Geosciences*, Vol. 36, No. 9, 1135–1144, 2010.

8. Warren, C. and A. Giannopoulos, "Creating finite-difference time-domain models of commercial ground-penetrating radar antennas using Taguchis optimization method," *Geophysics*, Vol. 76, No. 2, G37–G47, 2011.

9. Tillard, S. and J.-C. Dubois, "Analysis of GPR data: Wave propagation velocity determination," *Journal of Applied Geophysics*, Vol. 33, No. 1, 77–91, 1995.

10. Liu, H., X. Xie, and M. Sato, "Accurate thickness estimation of a backfill grouting layer behind shield tunnel lining by CMP measurement using GPR," *2012 14th International Conference on Ground Penetrating Radar (GPR)*, 137–142, IEEE, 2012.

11. Liu, H., K. Takahashi, and M. Sato, "Measurement of dielectric permittivity and thickness of snow and ice on a brackish lagoon using gpr," *IEEE Journal of Selected Topics in Applied Earth Observations and Remote Sensing*, Vol. 7, No. 3, 820–827, 2014.

12. Huang, Z. and J. Zhang, "Estimating properties of subsurface layers from GPR spectral attributes," *PIERS Proceedings*, 636–639, March 25–28, Taipei, 2013.

13. Huang, Z.-L. and J. Zhang, "Determination of parameters of subsurface layers using GPR spectral inversion method," Vol. 52, No. 12, 7527–7533, 2014.

14. Lambot, S., E. C. Slob, I. Van Den Bosch, B. Stockbroeckx, and M. Vanclooster, "Modeling of ground-penetrating radar for accurate characterization of subsurface electric properties," *IEEE Transactions on Geoscience and Remote Sensing*, Vol. 42, No. 11, 2555–2568, 2004.

15. Kalogeropoulos, A., J. Van Der Kruk, J. Hugenschmidt, J. Bikowski, and E. Brühwiler, "Full-waveform GPR inversion to assess chloride gradients in concrete," *Ndt & E International*, Vol. 57, 74–84, 2013.

16. Jonard, F., L. Weihermller, K. Z. Jadoon, M. Schwank, H. Vereecken, and S. Lambot, "Mapping field-scale soil moisture with l-band radiometer and ground-penetrating radar over bare soil," *IEEE Transactions on Geoscience and Remote Sensing*, Vol. 49, No. 8, 2863–2875, 2011.

17. Spagnolini, U., "Permittivity measurements of multilayered media with monostatic pulse radar," *IEEE Transactions on Geoscience and Remote Sensing*, Vol. 35, No. 2, 454–463, 1997.

18. Caorsi, S. and M. Stasolla, "A layer stripping approach for em reconstruction of stratified media," *IEEE Transactions on Geoscience and Remote Sensing*, Vol. 52, No. 9, 5855–5869, 2014.

19. Ardekani, M. R. M. and S. Lambot, "Full-wave calibration of time-and frequency-domain ground-penetrating radar in far-field conditions," *IEEE Transactions on Geoscience and Remote Sensing*, Vol. 52, No. 1, 664–678, 2014.

20. Debye, P. J. W., *Polar molecules*, Chemical Catalog Company, Incorporated, 1929.

21. Balanis, C. A., *Antenna Theory: Analysis and Design*, John Wiley & Sons, 2001.

22. Kong, J. A., *Theory of Electromagnetic Waves*, Vol. 1, 1975

23. Chew, W. C., *Waves and Fields in Inhomogeneous Media*, IEEE press, New York, 1995.

24. Dural, G. and M. I. Aksun, "Closed-form Green's functions for general sources and stratified media," *IEEE Transactions on Microwave Theory and Techniques*, Vol. 43, No. 7, 1545–1552, 1995.

25. Lambot, S., et al., "Hydrogeophysical characterization of soil using ground penetrating radar," Ph.D. Dissertation, Ph. D. Thesis, Catholic Univ. of Louvain, Louvain-la-Neuve, Belgium, 2003.

26. Jadoon, K. Z., S. Lambot, E. Slob, and H. Verrecken, "Investigation of the frequency dependent antenna transfer functions and phase center position for modeling off-ground GPR," *2010 13th International Conference on Ground Penetrating Radar (GPR)*, 1–7, IEEE, 2010.

27. Patriarca, C., M. Miorali, E. Slob, and S. Lambot, "Uncertainty quantification in off-ground monostatic ground penetrating radar," *IEEE Transactions on Antennas and Propagation*, Vol. 61, No. 6, 3334–3344, 2013.

28. Harrington, R. F., *Time-harmonic Electromagnetic Fields*, McGraw-Hill, 1961.